ELSEVIER

Chemical Geology 240 (2007) 260–279

CHEMICAL GEOLOGY
INCLUDING
ISOTOPE GEOSCIENCE

www.elsevier.com/locate/chemgeo

The origin of medium-K ankaramitic arc magmas from Lombok (Sunda arc, Indonesia): Mineral and melt inclusion evidence

Marlina A. Elburg [a,b,c,*], V.S. Kamenetsky [a,d], J.D. Foden [e], A. Sobolev [a]

[a] *Max-Planck Institut für Chemie, Postfach 3060, 55020 Mainz, Germany*
[b] *Faculty of Earth and Life Sciences, Free University, De Boelelaan 1085, Amsterdam, The Netherlands*
[c] *Department of Geology and Soil Science, Ghent University, Krijgslaan 281 S8, 9000 Ghent, Belgium*
[d] *Centre for Ore Deposit Research and School of Earth Sciences, University of Tasmania, Hobart, Tasmania 7001, Australia*
[e] *Department of Geology and Geophysics, Adelaide University, Adelaide SA 5005, Australia*

Received 18 July 2006; received in revised form 13 February 2007; accepted 14 February 2007

Editor: S.L. Goldstein

Abstract

High-calcium, nepheline-normative ankaramitic basalts (MgO > 10 wt.%, $CaO/Al_2O_3 > 1$) from Rinjani volcano, Lombok (Sunda arc, Indonesia) contain phenocrysts of clinopyroxene and olivine (Fo_{85-92}) with inclusions of spinel (Cr# 58–77) and crystallised melt. Olivine crystals have variable but on average low NiO (0.10–0.23 wt.%) and high CaO (0.22–0.35 wt.%) contents for their forsterite number. The CaO content of Fo_{89-91} olivine is negatively correlated with the Al_2O_3 content of enclosed spinel (9–15 wt.%) and positively correlated with the CaO/Al_2O_3 ratios of melt inclusions (0.9–1.5). Major and trace element patterns of melt inclusions are similar to that of the host rock, indicating that the magma could have formed by accumulation of small batches of melt, with compositions similar to the melt inclusions. The liquidus temperature of the magma was ~ 1275 °C, and its oxygen fugacity ≤ FMQ + 2.5. Correlations between K_2O, Zr, Th and LREE in the melt inclusions are interpreted to reflect variable degrees of melting of the source; correlations between Al_2O_3, Na_2O, Y and HREE are influenced by variations in the mineralogy of the source. The melts probably formed from a water-poor, clinopyroxene-rich mantle source.

Keywords: Arc magma; Subduction; Ankaramite; Melt inclusions; Olivine; Spinel

1. Introduction

It is increasingly accepted that arc magmas are a complex mixture of silicate liquid(s) and one or more populations of crystals, which are not necessarily in equilibrium with the melt in which they are entrained (Danyushevsky et al., 2002; Reubi et al., 2002; Dungan and Davidson, 2004; Davidson et al., 2005; Kamenetsky et al., 2006). This implies that most whole rock analyses are unlikely to represent liquid compositions, and that we need to find other ways to determine the chemical composition of subduction-related melts. Since fresh, quenched glasses are not always available, the method of choice over the past 10 years has been the study of melt inclusions (Kamenetsky and Clocchiatti, 1996; Sobolev, 1996; Michaud et al., 2000; Sobolev et al., 2000; De Hoog et al., 2001; Kent and Elliott, 2002; Cervantes and Wallace, 2003). Melt inclusions have

* Corresponding author. Department of Geology and Soil Science, Ghent University, Krijgslaan 281 S8, 9000 Ghent, Belgium.
E-mail address: Marlina.Elburg@UGent.be (M.A. Elburg).

0009-2541/$ - see front matter © 2007 Elsevier B.V. All rights reserved.
doi:10.1016/j.chemgeo.2007.02.015

proved particularly useful to determine the volatile content of magmas, since these components are degassed during eruption (Sisson and Layne, 1993; Sobolev and Chaussidon, 1996; Gurenko et al., 2005; Wallace, 2005); and to study the composition of primitive arc magmas, which seldom reach the Earth's surface without modification. However, the validity of the latter application has been challenged by Danyushevsky et al. (2004), who suggest that melt inclusions in primitive olivine (with more than 85 mol% forsterite), that had been thought to convey information about primary magmas, often record the compositions of melts which have been formed by localised reactions with pre-existing crystal mushes. If true, these compositions would not provide definitive information on primary magmas, but only about magma chamber processes. In this view, only melt inclusions from more evolved olivine phenocrysts can yield information on the composition of silicate liquids that have played an important role in the petrogenesis of subduction-related magmas. This interpretation would be a severe blow to the usefulness of melt inclusion studies to determine the composition of primary arc magmas, since these would never be contained in olivines with forsterite contents lower than 85 mol%.

In particular, melt inclusions with high CaO contents and high CaO/Al_2O_3 ratios, found within olivine crystals from subduction-related magmas, have been identified as reflecting local melting reactions (Danyushevsky et al., 2004) or post-entrapment modification (Gaetani et al., 2002). This fits well with the theory that high CaO/Al_2O_3 melts, such as ankaramites, are formed by remelting of lower crustal cumulates (Médard et al., 2006) but does not agree with the alternative ideas that ankaramites reflect melting of a CO_2-fluxed depleted mantle source (Green et al., 2004) or fractionated melts of a high-pressure picritic parental magma (Della-Pasqua and Varne, 1997).

To add to this discussion on the origin of ankaramites and the usefulness of melt inclusion studies, we have made a detailed study of some medium-K, nepheline-normative ankaramitic basalt samples from the island of Lombok (Indonesia), and the melt inclusions in their olivine crystals. A clear correlation is observed between compositions of the olivine, melt inclusions, and, where present, spinel grains enclosed within olivine. Moreover, the trace element patterns of the analysed melt inclusions show a clear resemblance to that of the whole rock. This suggests that, in the case of these magmas, the melt inclusions in forsterite-rich olivine crystals ($Fo_{89–91}$) represent melt batches whose mixing is responsible for generating the whole rock composition.

2. Geological background

The island of Lombok is part of the Indonesian Sunda arc (Fig. 1), and is built on crust whose thickness is transitional between continental and oceanic domains (depth to Moho about 20 km). Volcanic activity in the arc is a response to northward dipping subduction of the Australian plate. In the easternmost Sunda arc, this has led to collision between the arc and the Australian continent, but the crust subducted beneath Lombok is still oceanic in character. The active volcano on the island is Rinjani, which is located approximately 165 km above the Benioff zone. The samples studied are derived from lava flows exposed on the north–northeast coast of the island, near the village of Obel–Obel. Although their

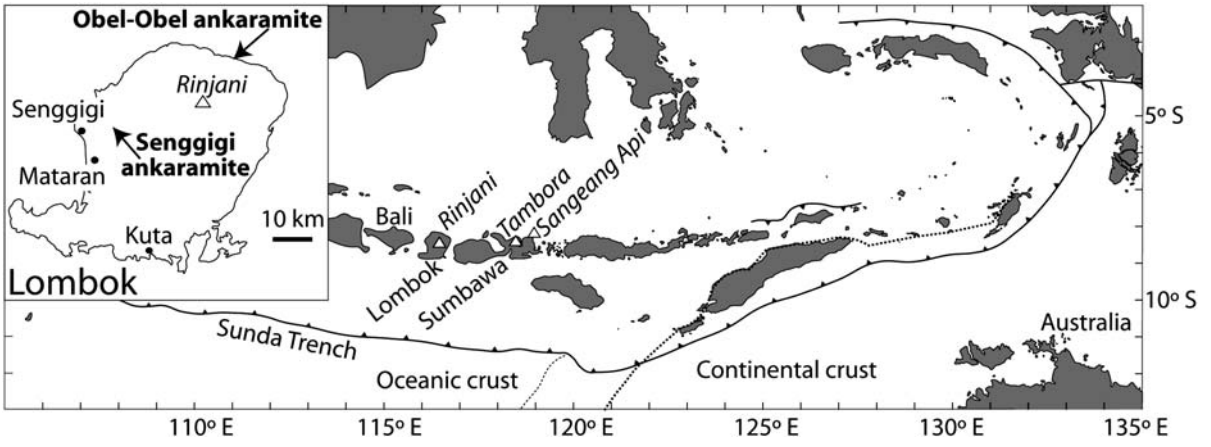

Fig. 1. Location of Lombok within the Indonesian arc, and location of the studied samples on Lombok (Obel–Obel ankaramite) and the Senggigi ankaramites studied by Della-Pasqua and Varne (1997) and Foden (1983).

age is not constrained, the lava flows originated from the active volcano of Rinjani, and are therefore likely to be significantly younger than 1 Ma.

Magmas of Rinjani volcano show typical 'calc-alkaline' or medium-K arc characteristics, with most samples having 50–68% SiO_2, 6–0.7% MgO, while K_2O contents increase from 1 to 4.3%. Rare samples with higher MgO contents have been found, and have already been described by Foden (1983). These have high CaO/Al_2O_3 ratios, up to 1.37 at MgO contents of 14% (Fig. 2), and contain large phenocrysts of clinopyroxene and olivine, typical for ankaramites. The ankaramitic samples described by Foden (1983) come from the northwest side of the island, not far from Senggigi, whereas the ones used here come from the area east of Obel–Obel (Fig. 1; S8°16.238′, E116°34.899′). The material collected by Foden (1983) was already the subject of a mineral and melt inclusion study by Della-Pasqua and Varne (1997). Samples from the Obel–Obel area show a range in MgO and CaO/Al_2O_3 contents (Fig. 2), and those used for this study are the two most MgO-rich samples from the suite, LB43 and LB39 (MgO 11.3 and 10.2 wt.% respectively, CaO/Al_2O_3 = 1.03). No mineralogical differences were found between these two samples, and the results, which were mainly obtained from LB43, are discussed together. Some comparisons are made with the whole rock composition of one of the more mafic, lower CaO/Al_2O_3 (i.e. "normal arc") samples from Rinjani volcano (LB23; Fig. 2). This sample comes from a flow in a river bed to the NE of the city of Mataran (S8°34.403′, E116°8.599′).

3. Analytical techniques

Major element mineral and glass analyses were performed on a JEOL 8200 electron microprobe at the Max Planck Institute for Chemistry, using natural mineral standards for calibration. Olivine and spinel were analysed with an accelerating voltage of 20 kV and a current of 20 nA. All other phases were analysed with 15 kV and 12 nA. The beam diameter was 2 μm. Sodium was always the first element to be measured, to avoid migration of this element away from the electron beam. To obtain paired analyses of olivines and melt inclusions, olivine analyses were performed at distances of approximately 30 μm from the melt inclusion to avoid NiO-depletion and CaO-enrichment of the olivine by diffusional exchange between the two phases. The accuracy of the analyses was assessed using the composition of the VG2 glass standard (USNM 111240/52) and San Carlos olivine (USNM 1113122/444) (Table 2). All paired glass–olivine analyses are averages of 2–3 individual analyses.

Trace elements in the melt inclusions were analysed by laser ablation ICP-MS, using a Finnigan Element 2 with a Merchantek 213 nm laser, and by Cameca 3f ion microprobe, both housed at the Max Planck Institute for Chemistry. LA-ICP-MS analyses were performed with He as carrier gas. The instrument was tuned to minimise oxide production, which was always less than 1% of the signal of its element. Raw Th/U ratios of the NIST 612 glass were ~ 0.91, compared to the real ratio of ~ 1, indicating that fractionation of the elements from each other during analysis was limited. The laser was operated with a spot size of 60 μm at 6 J/cm^2 and resulted in pits with height:width ratios of 1. One run consisted of 60 scans of 1.5 s each, of which the first 17 scans were taken with the laser shutter closed, to determine the blank, which was subtracted from the analysis. The analyses were normalised to the Ca content of the inclusion, which had been determined prior to laser ablation by electron microprobe. Melt inclusions with dimensions smaller than 60 μm were also analysed, in which case part of the enclosing olivine was ablated. This is unlikely to have affected either the relative or absolute trace element abundances measured for the melt inclusion significantly, since olivine has extremely low levels of all trace elements analysed, and very minor contents of the normalising element Ca. Not all scans were used for all inclusions, since the inclusion was sometimes thinner than 60 μm. In that case, only those scans were used where all elements were above the detection limit. NIST SRM612 glass was used for calibration, but was always analysed at the end of the complete set of analyses, to avoid memory effects for elements which are far lower in the glasses analysed than in the calibration standard (e.g. Ta, Nb, Hf). Secondary standards (KL2G and StHs6/80-G; Jochum

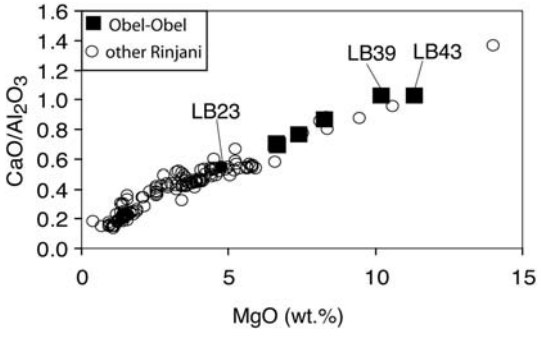

Fig. 2. CaO/Al_2O_3 versus MgO (wt.%) for whole rock samples from the island of Lombok. Circles: samples analysed by Foden (1983) and Foden, Elburg and Paraschivolu, (unpublished); squares: samples from the north-west coast of Lombok (near the village of Obel–Obel), belonging to a more calcic suite than most other Lombok samples.

et al., 2006) were used to check the precision and accuracy of the analyses (Table 2). Ion microprobe measurements of REE were performed following techniques described by Hellebrand et al. (2002). Some inclusions were also analysed for H_2O, TiO_2, Li and B contents by ion microprobe, following analytical techniques published by Gurenko et al. (2005).

Major and trace elements of whole rock sample LB43 and LB23 were analysed by X-ray fluorescence at the Department of Geology and Geophysics at the University of Adelaide, using techniques described by Elburg and Foden (1999).

Most Sr and all Nd whole rock isotopic ratios were analysed in the same Adelaide laboratory on a ThermoFinnigan MAT 262 thermal ionisation mass spectrometer, following procedures described by Elburg et al. (2003). The $^{143}Nd/^{144}Nd$ La Jolla standard yielded a value of 0.511843±9 (2 SD; $n=8$) and 0.511827±6 (2 SD; $n=5$) during the two periods of analysis, and all analysed samples were normalised to a value of 0.511860 for this standard. The SRM-987 $^{87}Sr/^{86}Sr$ standard yielded 0.710249±28 (2 SD; $n=6$); analysed samples were not normalised. Pb and some Sr isotopic ratios were measured at the Free University (Amsterdam), on a ThermoFinnigan Neptune MC-ICPMS and ThermoFinnigan MAT 262 TIMS respectively following procedures described by Elburg et al. (2005). The SRM-987 standard gave 0.710244±14 (2 SD; $n=4$) during this period. As a result of the technique used for Pb isotope analysis, NBS981 could not be used as a secondary standard, while available whole rock standards were found to be inhomogeneously contaminated (Elburg et al., 2005). The most reliable reference material was found to be JGS JB-2, which yielded $^{206}Pb/^{204}Pb$ 18.3427±12, $^{207}Pb/^{204}Pb$ 15.5624±11 and $^{208}Pb/^{204}Pb$ 38.2782±32 (2 SD; $n=9$).

4. Petrology

The phenocryst assemblages of the two analysed samples are very similar, and consist of abundant large (up to 1 cm) olivine and clinopyroxene crystals and scarce small (<0.5 mm) plagioclase crystals, set in a fine-grained groundmass of the same three minerals and Fe–Ti-oxide. Discontinuous and oscillatory zoning is common in the clinopyroxene crystals. Optical zoning is not evident in the olivine crystals, except when the rims appear to have been corroded and the crystals show reverse zoning. Melt inclusions and spinel grains are hosted by olivine and clinopyroxene crystals. The less Mg-rich samples from this suite contain a higher proportion of plagioclase crystals, and significantly less olivine. Representative mineral analyses can be found in Table 1.

4.1. Olivine

The forsterite content (Fo) of most olivine cores varies between 86 and 92 mol%, but the cores of phenocrysts with resorption features can be as low as Fo_{65}. Groundmass olivine ranges down to Fo_{48}. Olivine crystals with forsterite contents between 89 and 91 mol% show a range of CaO and NiO contents, which are negatively correlated with each other (Fig. 3; Table 3), but do not show a clear correlation with Fo-content. The largest group has low NiO (0.10–0.13%) and high CaO (0.33–0.35%) contents, but there is a spread towards higher NiO (up to 0.22%, two crystals with 0.37%) and lower CaO (down to 0.23%, two crystals with 0.20%). Within individual crystals, forsterite contents decrease in the outer 100 μm of the crystal, towards values around Fo_{80} at the rim. Most crystals also show an increase in CaO contents towards their rims. Zoning with respect to NiO is antithetic to the observed CaO zoning. Although the range in CaO and NiO contents appears to be a continuum, the olivine crystals have been divided into a high-calcium and a low-calcium group, with a boundary at 0.28% CaO. This is only for ease of discussion and graphical representation, without claiming the existence of a sharp division between these two groups. The NiO contents at a given forsterite% are generally lower than in non-ankaramitic arc lavas from Indonesia (Reubi et al., 2002), but compositions are similar to high-Ca, low-Ni olivines from other ankaramitic arc lavas (Portnyagin et al., 2005b; Kamenetsky et al., 2006).

4.2. Clinopyroxene

The ratio $Mg/(Mg+Fe_{tot})$ of the clinopyroxene crystals ranges from 0.72 to 0.92, with the great majority higher than 0.82. Cr_2O_3 contents increase with increasing $Mg/(Mg+Fe_{tot})$ ratio, but there is a large spread of Cr_2O_3 values at the higher end of the range, from 0.45 to 0.95 wt.%. This range in Cr_2O_3 contents at high magnesium contents does not correlate with any other element. Al_2O_3 (4–1 wt.%) and TiO_2 (0.5–0.1 wt.%) show tighter negative correlations with $Mg/(Mg+Fe_{tot})$.

4.3. Plagioclase

Plagioclase occurs only as small crystals, with An-contents typically between 80 and 90 mol%, although the value can go down to 70 near rims or cracks. FeO contents are around 0.8 wt.% and MgO between 0.05

Table 1
Representative mineral compositions, determined by electron microprobe

	olXIII olivine	olXIII spinel	ol4.2 olivine	ol4.2 spinel	ol13.2 olivine	ol13.2 spinel	cpxb 3	cpxd 2	cpxh 1	cpxi 1	Plg phenocryst	Plg phenocryst	Plg micro phenocryst	Plg micro phenocryst
SiO_2	40.71	0.31	40.06	0.06	39.56	0.05	52.70	52.15	53.23	49.84	45.76	48.06	49.55	51.72
TiO_2		0.51		0.57		0.57	0.16	0.23	0.12	0.66				
Al_2O_3	0.04	14.92	0.02	12.61	0.01	9.84	1.31	2.14	1.07	3.37	33.30	32.18	30.65	28.94
FeO	9.38	20.61	9.73	26.26	9.12	24.45	2.90	4.00	3.06	8.41	0.85	0.76	1.13	1.06
MnO	0.16	0.21	0.19	0.23	0.18	0.27	0.08	0.11	0.06	0.21				
MgO	49.63	14.96	48.73	12.62	49.24	12.49	17.56	16.74	17.58	14.71	0.07	0.08	0.12	0.07
CaO	0.26	0.01	0.28		0.35		23.55	23.06	23.31	21.51	17.76	16.14	14.73	12.86
Na_2O							0.12	0.20	0.12	0.39	1.35	2.28	3.01	3.69
K_2O							0.00	0.01	0.01	0.00	0.12	0.19	0.28	1.13
NiO	0.29	0.16	0.15	0.09	0.08	0.04								
Cr_2O_3	0.06	47.39	0.04	47.18	0.05	51.95	0.92	0.65	0.34	0.01				
Total	100.53	99.24	99.19	99.62	98.59	99.66	99.30	99.29	98.90	99.10	99.20	99.68	99.46	99.45
$Fe^{3+}/(Fe_{tot})$ calc.		0.42		0.42		0.39								
$100*Mg/(Mg+Fe^{2+})$	90.4	69.2	89.9	59.8	90.6	60.0								
$100*Mg/(Mg+Fe_{tot})$							91.5	88.2	91.1	75.7				
$100*Cr/(Cr+Al)$		68.1		71.5		78.0								
An											0.89	0.80	0.73	0.64
T (°C)		1196		1039		1038								
log fO_2 (Δ FMQ)		1.7		2.2		2.1								

Temperatures calculated following the method by Ballhaus et al. (1991a,b, 1994).

and 0.12 wt.%. Groundmass plagioclase contains 50–70 mol% An.

4.4. Spinel

Only spinel inclusions within olivine crystals were studied. These are typically chromium-rich spinel, with Mg# (= $100*Mg/(Mg+Fe^{2+})$) between 53 and 70, and Cr# (= $100*Cr/(Cr+Al)$) from 58 to 77. TiO_2 contents generally vary between 0.45 and 0.65 wt.%. Al_2O_3 varies between 9.5 and 15.6 wt.%. When only spinel grains within Fo>89 olivine crystals are considered, there is a negative correlation between the Al_2O_3 content of the spinel and the CaO content of the olivine (Fig. 4A), while the Cr# of the spinel is positively correlated with the olivine CaO content. The TiO_2 versus Al_2O_3 relationship of the spinel grains puts them within the lower end of the range for calc-alkaline and high-K volcanic arc spinel (Kamenetsky et al., 2001).

5. Melt inclusions

5.1. Melt inclusion description

Melt inclusions are present in all types of olivine crystals, and generally occur in an isolated fashion. Trails of inclusions, suggestive of healed cracks, have not been observed. All inclusions are crystallised to a fine mass, in which a vapour bubble sometimes could be observed. This necessitated the rehomogenisation of the inclusions before analysis (see below). The diameter of

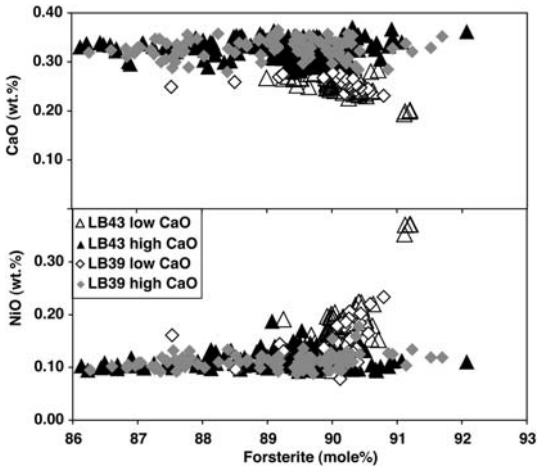

Fig. 3. CaO and NiO (wt.%) versus forsterite content of randomly selected olivine crystals from samples LB43 and LB39. Note the large spread of CaO and NiO at rather constant forsterite contents around Fo_{90}, and the antithetic behaviour of these two oxides.

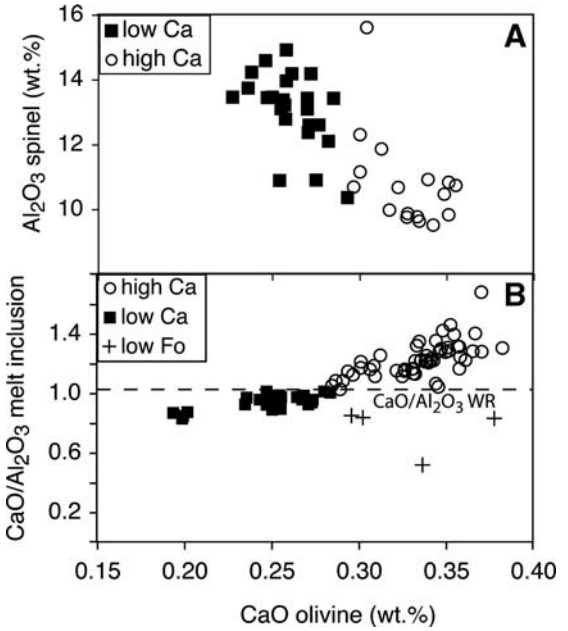

Fig. 4. A: Diagram showing the negative correlation of Al_2O_3 (wt.%) in spinel versus CaO (wt.%) of enclosing olivine ($Fo_{89–91}$). The positive correlation of Cr_2O_3 in spinel with CaO in olivine is less well defined. B: CaO/Al_2O_3 ratio of melt inclusions versus CaO content (wt.%) of enclosing olivine. There is a good correlation between these two parameters, apart from the inclusions within olivine with lower forsterite contents (crosses). These inclusions are not in equilibrium with their host olivine (see text for discussion). The dashed line indicates the CaO/Al_2O_3 ratio of the host rock.

the analysed inclusions varies from 20 to 160 μm, and is not related to the composition of the enclosing olivine. The size of the gas bubble within the rehomogenised inclusions is also independent of the size of the inclusion, suggestive of heterogeneous trapping of melt and vapour rather than exsolution of a vapour phase from the melt after trapping. Inclusions containing only a gas bubble are also observed.

All inclusions were rehomogenised in bulk, and visually controlled heating experiment were not performed. Olivine grains with unbreached melt inclusions were selected using a stereo microscope and were wrapped in Pt-foil or put into Pt-tubing for reheating, either in a gas-mixing furnace at the University of Heidelberg ($CO:CO_2 = 9:1$), or under Ar atmosphere at Hobart University (Tasmania, Australia). They were held at a temperature of 1250 °C for 3 to 10 min, and then quenched in water. After mounting in epoxy, the olivines were polished to expose the melt inclusions.

The rehomogenised inclusions consist of a colourless to brown glass and a vapour bubble of variable size. Some also contain a spinel inclusion, which can vary in size from a very small platelet at the wall of the inclusions to a crystal that takes up more than 90% of the volume of the inclusion. The latter type of inclusion was not analysed.

5.2. Major elements

Overall, there is a good correlation between the CaO content of the enclosing olivine and the CaO/Al_2O_3 ratio of the melt inclusion (Fig. 4B). Four analyses that fall clearly off the trend were measured within olivine phenocrysts with Fo contents lower than 84%, whereas all others were measured in Fo > 85 olivine. The inclusions in Fo < 84 olivine are also characterised by elevated FeO contents. This is most pronounced for the two inclusions measured in an olivine crystal with less than 70% Fo; these have FeO > 20 wt.% (Table 2). We interpret this Fe-enrichment to have been caused by an effect opposite to that of the Fe-loss phenomenon described by Danyushevsky et al. (2000) and Gaetani and Watson (2002). Fe-loss is caused by sidewall crystallisation of olivine, which causes an increase of the Fe/Mg ratio of the residual melt within a melt inclusion; this high Fe/Mg liquid then equilibrates with the 'infinite reservoir' of high-Fo (= low Fe/Mg) olivine. In our case, low-Fo olivine was partially dissolved during entrainment in hot, high-Mg magma, whereby droplets of low Fe/Mg melt became included in olivine with a lower-Fo-content (= higher Fe/Mg ratio) than its equilibrium olivine. Equilibration of the melt with this olivine then caused a pronounced increase in the Fe/Mg ratio of the melt, and led to excessively high FeO* contents in the rehomogenised melt inclusion. That this process has taken place can also be judged from the high-Fo (low-Fe) olivine rim around these melt inclusions (Fig. 5). Since the included melt and the olivine were not in equilibrium with each other, these inclusions will be excluded from further discussion.

Trends of decreasing olivine Fo-content towards melt inclusions (with normal Fe-contents) were observed in some of the high-Fo olivine crystals (not shown), indicating that the process of iron-loss must have occurred. To reverse this process mathematically, the method of Danyushevsky et al. (2000) was followed for melt inclusions in $Fo_{89–91}$ olivines, using the olivine–melt equilibrium model of Ford et al. (1983). We limit the remainder of the paper to the discussion of melt inclusions in these most Fo-rich olivines, to focus on trends in the most primitive liquids, unrelated to fractional crystallisation. The initial FeO-content of the melt was assumed to have been 9.6 wt.%, similar to that of the host rock. Considering the trends observed in

Table 2
Analyses of melt inclusions (no Fe-loss correction) and enclosing olivines, whole rocks (LB43 WR, LB23 WR), olivine and glass microprobe standards (SC, VG2), trace element standards (StHs6/80-G, KL2-G), and their recommended values (Jochum et al., 2006)

Sample	LB43 ol2	LB43 ol4	LB43 ol13-1	LB43 ol13-2	LB43 ol23	LB43 ol43	LB43 ol49	LB43 ol48	LB43 ol51	LB43 ol52-1	LB43 ol52-2
SiO_2	46.09	46.42	44.79	44.86	45.85	45.80	43.95	44.57	45.44	46.23	46.18
TiO_2	0.79	0.84	1.21	1.22	0.90	0.99	1.39	0.92	0.81	0.82	0.86
Al_2O_3	14.19	17.38	18.44	18.43	13.62	11.85	13.90	15.94	13.85	12.61	13.19
FeO	8.59	5.79	6.31	6.48	7.56	12.31	8.24	7.21	7.60	7.33	7.24
MnO	0.17	0.09	0.09	0.09	0.13	0.18	0.14	0.13	0.14	0.15	0.15
MgO	9.37	8.52	8.36	8.14	9.48	10.18	9.63	10.11	10.39	11.04	10.52
CaO	15.87	15.49	15.36	15.67	17.51	16.90	16.94	16.17	16.82	16.58	17.47
Na_2O	2.53	3.16	3.38	3.30	2.32	1.14	2.04	2.75	2.24	2.05	2.12
K_2O	0.92	0.88	1.22	1.20	0.85	0.21	1.58	1.07	0.83	1.03	1.14
P_2O_5	0.11	0.12	0.23	0.23	0.12	0.08	0.69	0.15	0.12	0.17	0.20
Cl	0.15	0.16	0.28	0.28	0.14	0.06	0.09	0.17	0.13	0.13	0.15
S	0.13	0.10	0.17	0.18	0.13	0.01	0.14	0.15	0.15	0.10	0.13
F						0.01	0.00	0.00	0.01	0.01	0.02
Total	98.87	98.91	99.76	100.01	98.58	99.69	98.72	99.30	98.48	98.21	99.33
mg#	66.0	72.4	70.2	69.1	69.1	59.6	67.6	71.4	70.9	72.9	72.1
CaO/Al_2O_3	1.12	0.89	0.83	0.85	1.29	1.43	1.22	1.01	1.21	1.31	1.33
Cs	0.48	0.47	0.44	0.41	0.39	0.15	0.94	0.49	0.33	0.60	0.51
Rb	15.7	14.5	24.4	25.6	13.8	5.9	29.4	17.4	12.6	19.6	18.5
Ba	303	290	175	173	253	20	398	398	262	1805	291
Th	1.4	1.6	1.6	2.0	1.2	1.2	2.9	1.7	1.0	2.0	2.1
U	0.31	0.45	0.27	0.29	0.31	0.18	0.60	0.42	0.27	0.45	0.50
Nb	1.4	1.0	2.3	2.3	1.2	1.2	3.4	1.8	1.6	2.5	2.8
Ta	0.09	0.07	0.15	0.11	0.09	0.12	0.26	0.13	0.11	0.19	0.20
La	7.1	8.3	6.8	6.8	6.2	5.8	13.5	8.8	6.1	11.4	11.9
Ce	13.9	15.2	15.0	15.2	13.0	9.9	26.4	17.4	12.3	21.2	22.5
Pb	3.7	3.9	3.5	7.4	3.9	5.2	5.4	3.6	2.4	3.3	3.7
Pr	1.9	2.1	2.0	2.2	1.7	1.6	3.2	2.4	1.7	2.9	2.8
Sr	466	561	380	397	447	219	523	551	381	585	555
Nd	9.4	10.1	10.0	10.9	8.3	7.5	13.8	11.4	8.7	13.1	12.6
Sm	2.6	2.8	2.7	3.1	2.0	2.0	3.1	3.1	2.2	2.7	2.9
Zr	40.0	41.1	56.0	59.5	34.4	88.2	61.8	46.2	34.3	42.6	43.9
Hf	1.31	1.16	1.70	1.58	1.15	2.15	1.56	1.52	1.10	1.45	1.43
Eu	0.77	1.02	0.92	1.11	0.82	0.81	0.60	1.01	0.76	0.86	0.90
Gd	2.8	3.2	3.2	3.4	2.5	2.9	2.8	3.4	2.5	2.8	2.8
Tb	0.48	0.51	0.58	0.52	0.39	0.51	0.33	0.53	0.37	0.38	0.39
Dy	3.0	3.3	3.5	4.4	2.8	3.7	2.3	3.4	2.3	2.3	2.5
Y	15.6	18.5	20.0	21.0	14.3	23.3	12.9	17.8	13.4	14.3	13.0
Ho	0.61	0.68	0.78	0.88	0.58	0.80	0.44	0.74	0.51	0.54	0.52
Er	1.77	1.99	1.99	2.12	1.53	2.23	1.60	1.96	1.30	1.42	1.40
Tm	0.24	0.27	0.30	0.32	0.20	0.33	0.19	0.29	0.21	0.19	0.21
Yb	1.61	1.79	2.38	1.74	1.48	2.19	2.06	1.99	1.43	1.43	1.52
Lu	0.25	0.29	0.26	0.31	0.23	0.32	0.23	0.28	0.22	0.19	0.21
H_2O%											
Li ppm											
B ppm											
SiO_2 ol	40.20	39.63	40.20	40.48	40.62	40.47	40.80	41.17	40.86	41.00	40.98
Al_2O_3 ol	0.03	0.03	0.04	0.03	0.02	0.03	0.02	0.03	0.01	0.01	0.02
FeO ol	10.53	9.52	8.55	8.51	10.03	12.86	11.05	9.09	10.73	9.49	9.31
MnO ol	0.20	0.18	0.15	0.15	0.20	0.23	0.19	0.19	0.18	0.18	0.16
MgO ol	48.21	47.99	49.28	49.45	48.34	47.00	48.50	49.80	48.68	49.48	49.66
CaO ol	0.32	0.25	0.20	0.20	0.37	0.35	0.34	0.28	0.34	0.36	0.33
NiO ol	0.12	0.20	0.37	0.37	0.11	0.10	0.10	0.15	0.11	0.11	0.10
Cr_2O_3 ol	0.02	0.04	0.05	0.05	0.03						
Total ol	99.63	97.84	98.84	99.25	99.71	101.04	101.00	100.70	100.92	100.63	100.55
Fo ol	89.1	90.0	91.1	91.2	89.6	86.7	88.7	90.7	89.0	90.3	90.5

Table 2 (*continued*)

Sample	LB43 ol54	LB43 ol61	LB43 ol48	LB43 ol21	LB43 ol4-2	LB43 ol7	LB43 ol9-2	LB43 ol23	LB43 ol42	LB43 ol44	LB43 ol46-1
SiO_2	45.31	47.14	45.75	45.84	47.24	44.69	45.82	45.13	45.73	50.01	45.73
TiO_2	1.19	0.79	1.09	1.09	0.77	1.42	0.77	0.98	1.01	1.14	0.87
Al_2O_3	17.39	15.43	16.36	16.15	16.80	14.18	15.97	13.78	14.36	11.21	14.34
FeO	6.92	5.95	5.69	7.29	5.70	8.36	7.30	7.76	7.94	10.64	7.08
MnO	0.12	0.10	0.09	0.09	0.10	0.13	0.12	0.14	0.13	0.19	0.15
MgO	9.75	10.04	9.71	9.50	9.27	9.11	9.39	9.36	10.21	10.27	9.88
CaO	15.14	15.01	16.47	15.89	15.60	17.37	15.59	17.67	16.88	12.91	17.56
Na_2O	3.36	2.73	3.03	2.51	2.89	2.29	2.57	2.29	2.34	1.53	2.33
K_2O	1.23	0.80	1.23	0.84	0.85	1.06	0.82	0.83	0.82	0.68	0.83
P_2O_5	0.22	0.14	0.18	0.14	0.11	0.17	0.12	0.16	0.18	0.23	0.14
Cl	0.26	0.10	0.20	0.16	0.15	0.14	0.14	0.15	0.13	0.01	0.14
S	0.13	0.09	0.13	0.13	0.11	0.16	0.13	0.11	0.13	0.02	0.15
F	0.01	0.01	0.01	0.00	0.01		0.00	0.00	0.01	0.03	0.01
Total	100.97	98.30	99.88	99.59	99.57	99.06	98.69	98.32	99.85	98.84	99.16
mg#	71.5	75.0	75.2	69.9	74.3	66.0	69.6	68.2	69.6	63.2	71.3
CaO/Al_2O_3	0.87	0.97	1.01	0.98	0.93	1.23	0.98	1.28	1.18	1.15	1.22
Cs	0.49	0.29	0.40	0.42							
Rb	27.7	13.7	19.4	13.6							
Ba	210	247	416	269							
Th	1.4	1.0	1.9	1.4							
U	0.32	0.29	0.41	0.31							
Nb	4.0	2.1	1.8	1.7							
Ta	0.27	0.09	0.10	0.10							
La	9.3	5.9	9.0	7.8							
Ce	19.8	11.9	18.9	16.2							
Pb	2.0	2.5	5.0	3.0							
Pr	2.8	1.6	2.5	2.2							
Sr	438	348	594	478							
Nd	13.5	7.4	12.7	10.8							
Sm	3.7	2.6	3.0	2.9							
Zr	64.9	32.8	49.1	40.8							
Hf	1.91	0.85	1.55	1.21							
Eu	1.21	0.87	1.04	0.93							
Gd	4.4	3.0	3.7	3.0							
Tb	0.63	0.42	0.53	0.45							
Dy	4.4	3.3	3.3	2.9							
Y	21.7	15.8	18.5	16.2							
Ho	0.86	0.53	0.71	0.60							
Er	2.39	1.48	2.09	1.66							
Tm	0.32	0.19	0.29	0.26							
Yb	2.24	1.75	1.89	1.81							
Lu	0.33	0.25	0.26	0.25							
H_2O%	0.09				0.11	0.04	0.03	0.01	0.09	0.04	0.02
Li ppm	4.50				3.64	2.71	4.69	3.18	3.80	18.15	3.00
B ppm	11.16				9.50	4.55	8.07	8.80	9.21	178.9	7.68
SiO_2 ol	41.10	41.26	41.17	40.72	40.32	40.29	40.89	40.25	40.92	41.00	41.12
Al_2O_3 ol	0.04	0.03	0.03	0.04	0.03	0.02	0.02	0.04	0.03	0.02	0.02
FeO ol	8.70	9.33	9.09	9.73	9.64	10.11	9.57	10.17	10.14	11.26	10.93
MnO ol	0.14	0.18	0.19	0.18	0.18	0.21	0.18	0.20	0.18	0.21	0.20
MgO ol	50.02	49.97	49.80	49.01	49.58	48.47	49.79	48.49	49.52	48.50	48.91
CaO ol	0.19	0.24	0.28	0.25	0.27	0.36	0.26	0.37	0.30	0.33	0.33
NiO ol	0.35	0.19	0.15	0.19	0.20	0.11	0.18	0.10	0.11	0.10	0.11
Cr_2O_3 ol					0.04	0.03	0.04	0.02			
Total ol	100.54	101.18	100.70	100.14	100.26	99.60	100.93	99.65	101.19	101.41	101.61
Fo ol	91.11	90.52	90.71	89.98	90.17	89.52	90.26	89.57	89.69	88.47	88.81
Li ol	1.22					1.40		1.52	1.25		
B ol	0.18					0.30		0.43	0.20		

(continued on next page)

Table 2 (*continued*)

Sample	LB43 ol50	LB43 ol53	LB43 ol56	LB43 ol31-1	LB39 ol406	LB39 ol401	LB39 ol403	LB39 ol407	VG2, SC olivine(1 SD)	LB43 WR	LB23 WR
SiO_2	45.98	45.42	46.53	44.06	47.55	47.24	46.30	46.42	50.7 (0.27)	47.70	51.76
TiO_2	0.85	0.87	0.74	0.46	0.70	0.78	0.81	0.83	1.87 (0.02)	0.78	1.16
Al_2O_3	13.02	13.65	13.25	17.54	15.15	13.76	16.18	15.92	14.12 (0.07)	12.53	17.43
FeO	7.64	7.38	8.20	20.18	6.96	7.54	6.66	6.28	11.8 (0.16)	9.56	8.83
MnO	0.15	0.13	0.11	0.39	0.10	0.12	0.11	0.10	0.21 (0.02)	0.18	0.16
MgO	10.44	9.96	11.54	6.26	10.40	10.10	9.84	10.01	6.6 (0.10)	11.31	4.87
CaO	17.61	17.87	16.11	9.06	16.47	17.60	15.04	15.30	10.92 (0.07)	12.93	9.88
Na_2O	2.27	2.22	2.01	2.02	2.19	2.20	2.80	2.72	2.84 (0.05)	2.02	3.11
K_2O	0.93	0.88	0.74	0.76	0.74	0.81	1.04	0.71	0.20 (0.01)	0.93	1.81
P_2O_5	0.18	0.14	0.10	0.14	0.11	0.12	0.17	0.11	0.22 (0.02)	0.16	0.30
Cl	0.13	0.17	0.15	0.04	0.15	0.14	0.14	0.17	0.033 (0.002)		
S	0.13	0.16	0.13	0.01	0.12	0.14	0.11	0.10	0.14 (0.01)		
F	0.00	0.00	0.00	0.00	0.00	0.00	0.02	0.00			
Total	99.30	98.82	99.58	100.92	100.60	100.52	99.17	98.63		100.00	100.14
mg#	70.9	70.6	71.5	35.6	72.7	70.5	72.5	74.0		67.8	49.6
CaO/Al_2O_3	1.35	1.31	1.22	0.52	1.09	1.28	0.93	0.96		1.03	0.57
Cs						0.41	0.39	0.26		0.2	
Rb						14.4	18.1	11.4		20.8	49.1
Ba						280	294	241		405	481
Th						1.2	1.6	1.0		1.62	5.7
U						0.29	0.37	0.25		0.36	1.39
Nb						1.3	2.3	1.0		2.4	7.7
Ta						0.09	0.15	0.08		0.15	
La						6.7	8.0	5.2		9,0	17.5
Ce						13.6	15.2	10.9		17.3	43
Pb						2.9	3.8	2.5		3.7	9.7
Pr						1.9	2.0	1.7		2.4	4.6
Sr						457	463	376		441	511
Nd						9.2	9.6	8.1		10.7	19.9
Sm						2.6	2.3	2.2		2.8	4.8
Zr						38.2	39.6	30.6		48.5	149.3
Hf						1.19	1.10	1.00		1.35	3.63
Eu						0.84	0.76	0.79		0.93	1.39
Gd						2.8	2.5	2.8		3.1	5.01
Tb						0.42	0.44	0.47		0.47	0.76
Dy						2.8	2.6	3.0		2.9	4.85
Y						15.2	16.5	15.7		17.8	30.3
Ho						0.58	0.53	0.59		0.58	0.97
Er						1.61	1.59	1.79		1.67	2.86
Tm						0.25	0.21	0.28		0.25	0.42
Yb						1.62	1.63	1.71		1.55	2.64
Lu						0.24	0.24	0.25		0.22	0.39
H_2O%	0.03	0.03	0.73		0.27						
Li ppm	3.05	2.83	3.97		3.07						
B ppm	9.74	8.60	7.64		7.44						
SiO_2 ol	40.98	40.99	40.98	37.45	40.94	40.27	40.96	40.97	40.6 (0.25)		
Al_2O_3 ol	0.02	0.02	0.02	0.03	0.02	0.02	0.05	0.04	0.03 (0.01)		
FeO ol	10.08	10.57	10.33	29.29	9.88	11.34	9.79	9.84	9.50 (0.06)		
MnO ol	0.18	0.20	0.22	0.61	0.19	0.21	0.18	0.19	0.14 (0.01)		
MgO ol	49.15	49.04	48.81	33.82	49.16	47.52	49.26	49.53	49.0 (0.3)		
CaO ol	0.33	0.38	0.30	0.34	0.29	0.35	0.25	0.24	0.09 (0.01)		
NiO ol	0.09	0.10	0.14	0.04	0.11	0.11	0.18	0.20	0.37 (0.004)		
Cr_2O_3 ol				0.00					0.01 (0.01)		
Total ol	100.83	101.29	100.79	101.57	100.58	99.82	100.66	101.00			
Fo ol	89.7	89.2	89.4	67.3	89.9	88.2	90.0	90.0			
Li ol			1.58								
B ol			0.16								

Table 2 (*continued*)

Sample	StHs6/80-G	1 SD	StHs6/80-G recommended	KL2-G	1 SD	KL2-G recommended
Cs	1.34	0.05	1.75	0.10	0.02	0.115
Rb	25.24	0.81	30.7	7.97	0.19	8.7
Ba	273.27	2.47	298	111.17	3.02	123
Th	2.35	0.14	2.28	1.01	0.04	1.02
U	0.82	0.06	1.01	0.46	0.03	0.548
Nb	6.13	0.12	6.94	14.21	0.26	15
Ta	0.42	0.02	0.42	1.00	0.04	0.961
La	12.12	0.14	12	13.17	0.35	13.1
Ce	24.00	0.32	26.1	30.56	0.68	32.4
Pb	9.00	0.76	10.3	2.35	0.79	2.07
Pr	3.07	0.05	3.2	4.45	0.11	4.6
Sr	472.26	7.65	482	337.95	5.24	356
Nd	12.98	0.24	13	21.46	0.62	21.6
Sm	2.79	0.09	2.78	5.51	0.15	5.54
Zr	118.64	1.55	118	144.70	3.29	152
Hf	3.11	0.09	3.07	3.93	0.14	3.93
Eu	0.91	0.01	0.953	1.84	0.06	1.92
Gd	2.63	0.09	2.59	6.03	0.28	5.92
Tb	0.38	0.01	0.371	0.87	0.04	0.89
Dy	2.32	0.10	2.22	5.40	0.22	5.22
Y	12.19	0.11	11.4	25.30	0.88	25.4
Ho	0.45	0.02	0.42	1.01	0.04	961
Er	1.25	0.03	1.18	2.59	0.13	2.54
Tm	0.18	0.00	0.172	0.34	0.02	0.331
Yb	1.21	0.07	1.13	2.17	0.12	2.1
Lu	0.18	0.01	0.168	0.30	0.02	0.285

Mg# = 100 * Mg / (Mg + Fe_{tot}).

CaO, Al_2O_3 and Na_2O in the melt inclusions, it is probable that the iron content would have varied between inclusions, and this assumption of a fixed iron content is therefore an oversimplification. The recalculation showed slight underheating of the melt inclusions at 1250 °C, which was corrected for by adding up to 15% of olivine to the analysis. This recalculation process does not affect the trends seen in elements that are incompatible in olivine, such as Al, Na and Ca. The variation in CaO/Al_2O_3 ratios reflects the roughly antithetic behaviour of these two oxides within the melt inclusions. The Al_2O_3 contents of the inclusions show a clear positive correlation with their Na_2O contents (Fig. 6; Table 3), but there are a few inclusions with anomalously low Na_2O contents of <1.7 wt.%, contrasting with the 2–3.4 wt.% range for the other inclusions.

The SiO_2 content of most glass inclusions varies between 44 and 48 wt.% (Table 2), irrespective of the Fo or CaO content of the enclosing olivine. All melt inclusions are nepheline-normative. The K_2O contents of the melt inclusions are not correlated with CaO, but a discernible positive correlation exists with P_2O_5 content (Fig. 6). The composition of the five melt inclusions from Lombok ankaramitic samples published by Della-Pasqua and Varne (1997) fall within the range of the inclusions measured in this study; four out of their five analysed inclusions have compositions within our group of low-Ca olivine-hosted inclusions. In terms of major elements, the inclusions are similar to those found in magnesian olivines from Avachinsky Volcano in Kamchatka (Portnyagin et al., 2005a) and from Batan Island in the Luzon–Taiwan arc (Schiano et al., 2000).

5.3. Volatiles and trace elements

Cl and S contents hover around 0.15 wt.%; the inclusions in the olivines with the lowest Ca contents have the highest Cl contents (0.26–0.29 wt.%). F contents are always lower than 0.04 wt.% and often below the detection limit of the microprobe measurements (0.004 wt.%). Water contents of the glasses are low. One inclusion gave a reproducible concentration of 0.7 wt.%, one 0.27 wt.%, but the other ten inclusions that were measured varied between 0.01 and 0.11 wt.%. This is unlikely to reflect water loss during rehomogenisation, because of short experimental heating times. Carbon was not analysed in the glass, but bubbles within inclusions and gas bubbles that were not associated with melt inclusions yielded a clear CO_2 signal,

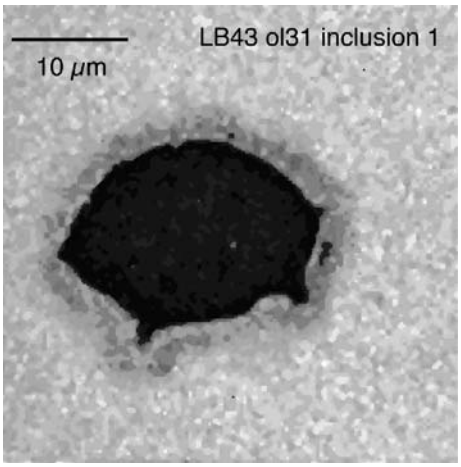

Fig. 5. Electron microprobe map of Fe-contents in and around melt inclusion in low-Fo olivine. The darker colours reflect lower Fe-contents. The olivine away from the inclusion contains 29.3% FeO and the inclusion itself 20.2%. The depletion in Fe of the olivine around the inclusion is interpreted as reflecting diffusive Fe–Mg-exchange with the initially low Fe/Mg glass.

with a trace of N_2 (approximately 1%) by Raman micro-spectroscopy.

The N-MORB normalised trace element patterns of most inclusions are quite consistent, and resemble that of the whole rock (Fig. 7). The patterns display pronounced negative anomalies for Nb–Ta and Ti, and positive anomalies for K, Pb and Sr, as is common for subduction-related magmas. The normalised trace element patterns are broadly similar to that of the non-ankaramitic lavas from Lombok, such as sample LB23 (Fig. 7). Chondrite normalised Rare Earth Element patterns are quite flat, with $(La/Lu)_{ch}=2–6$ and $(Gd/Lu)_{ch}=1.1–1.8$ (not shown). The one low-Na inclusion analysed has an aberrant trace element pattern,

Table 3
Summary of the two contrasting trends between $Fo_{89–91}$ olivines, enclosed spinel and melt inclusions

	Trend 1 (with K_2O MI)	Trend 2 (with CaO olivine)
Olivine Fo	0	0
Olivine CaO	0	Determinant
Olivine NiO	0	−
Spinel Al_2O_3	0	−
Spinel Cr_2O_3	0	Scattered+
MI Al_2O_3	0	−
MI CaO	0	+
MI Na_2O	0	−
MI K_2O	Determinant	0
Mi Li	0	−
MI Rb	+	0
MI Th	+	0
MI Zr	+	0
MI Y	0	−
MI LREE	+	0
MI HREE	0	−
MI Ni	0	−
calculated Interpretation	% Partial melting	Source mineralogy

Trend 1 is determined by the K_2O content of the melt inclusions, trend 2 by the CaO content of the enclosing olivine. + = positive correlation; − = negative correlation; 0 = no correlation.

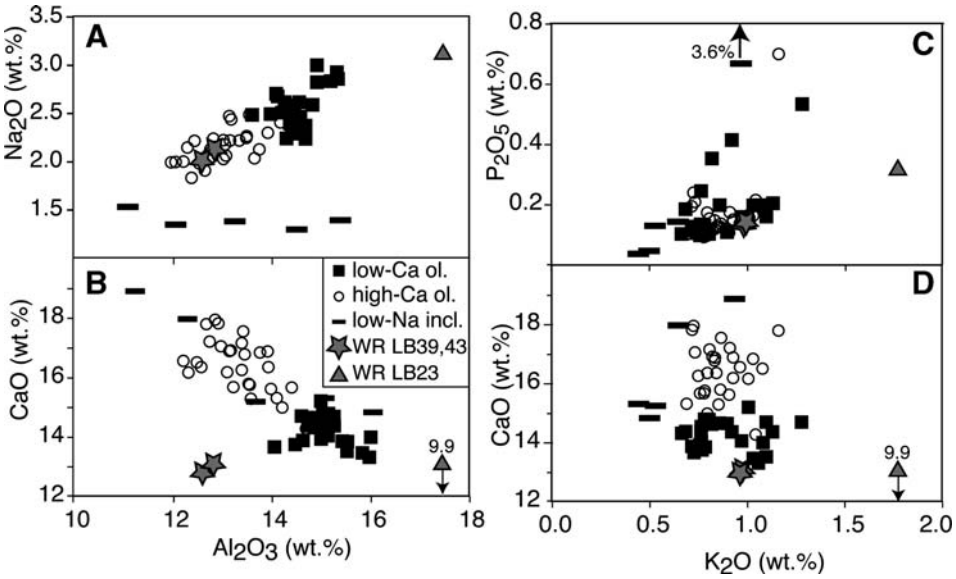

Fig. 6. A, B: Na_2O and CaO (A, B) contents (wt.%) against Al_2O_3 (wt.%) for (FeO-loss corrected) melt inclusions in $Fo_{89–91}$ olivine crystals, and whole rocks. C, D: CaO and P_2O_5 versus K_2O for the same melt inclusions and whole rocks. No correlation exists between calcium and potassium, contrasting with the better correlation with phosphorus (albeit with a subtrend towards higher P_2O_5 contents).

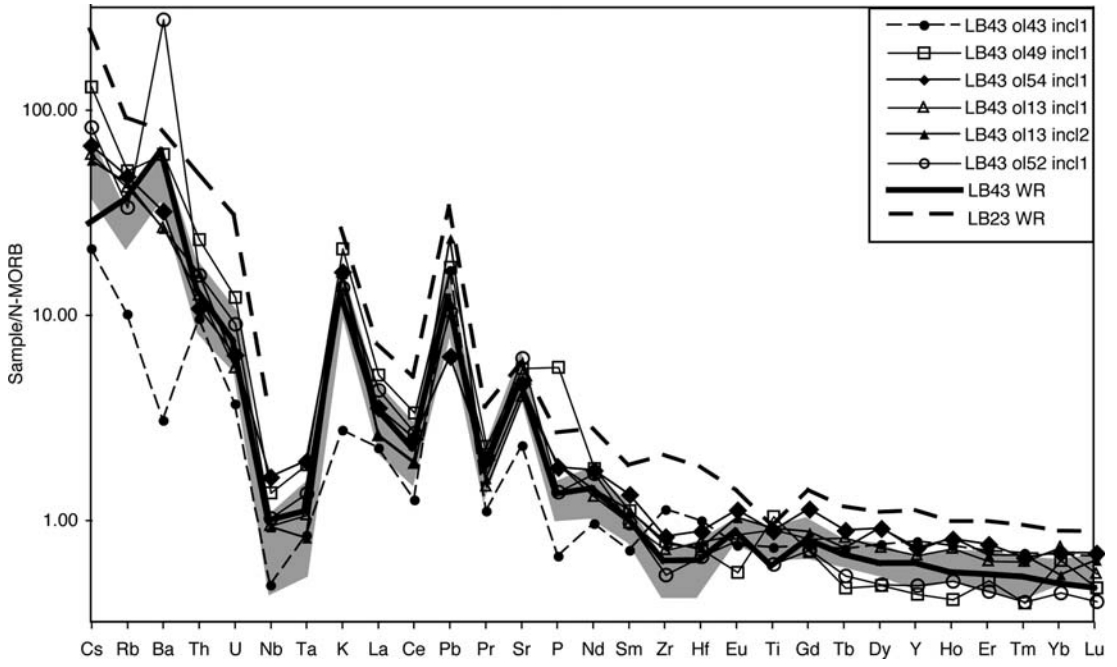

Fig. 7. N-MORB normalised incompatible element patterns for inclusions and whole rock analyses for LB43 and LB23. The patterns for the whole rock and melt inclusions are very similar (the lower Cs contents of the whole rock is likely to reflect mild alteration of the groundmass). The grey area is the field for 13 inclusions from LB43 (9) and LB39 (3) that show a close resemblance to each other (outlying Ba analysis (Table 2) not incorporated in the field). The three inclusions analysed in Ni-rich (0.35–0.27 wt.%) olivines 54 and 13 do not show the same negative Rb anomaly as the others. The inclusion in olivine 43 has anomalous low Na and volatile content, suggesting it may have been breached. Normalising values from Sun and McDonough (1989). LB23 is one of the more mafic non-ankaramitic samples from Rinjani volcano (4.9% MgO, 51.8% SiO_2) for which trace element data are available.

with significantly lower values for most Large Ion Lithophile Elements (LILE). We do not know what caused the low Na_2O content in some inclusions, but we notice that 4 of the 5 low-Na inclusions also show reduced contents of Cl and S. This, together with the unusual trace element composition, suggests that these inclusions may have been breached and that their low Na_2O contents are not a primary feature. We will therefore not consider these low-Na inclusions further. Most inclusions have lower MORB-normalised values for Rb than for Ba, but the three inclusions in the two most Ni-rich olivines (13 and 54) show a smooth increase from Rb through Ba to Cs.

There is a good positive correlation between many incompatible elements, irrespective of the Ca-content of the melt inclusion or its enclosing olivine (Fig. 8; Table 3). K_2O correlates with Rb, Th, the LREE and Zr, elements that show different geochemical behaviour in terms of fluid mobility (and which were analysed by different analytical methods). The correlation with Ba and Sr is poorer (these elements however correlate with each other). The HREE, Y and, to a lesser extent, Li content of the melt inclusions correlate with their Na_2O and Al_2O_3 contents (Fig. 8; Table 3).

6. Discussion

6.1. Olivine, spinel and melt inclusion correlations

The compositions of the $Fo_{89–91}$ olivine crystals and those of enclosed spinel grains and melt inclusions show clear and consistent correlations. There is a positive correlation between the CaO content of olivines and melt inclusions (Fig. 4B), whereas the Al_2O_3 content of melt inclusions and spinel correlates antithetically with the CaO content of enclosing olivine (Fig. 4A; Table 3). Since the Al-contents of the enclosing olivine are very low (<0.05 wt.%), it is not possible that the latter trend reflects post-entrapment re-equilibration between spinel and olivine. The good major element correlations between spinel, olivine and melt inclusions show that they are related to each other, and we propose that the olivine and spinel crystallised from melts similar to those represented by the associated melt inclusions.

Gaetani et al. (2002) have suggested that high-calcium contents of melt inclusions within olivine could be explained by diffusion of this element through the olivine lattice. Their model was developed in order to explain the high-calcium content of a low-Na melt

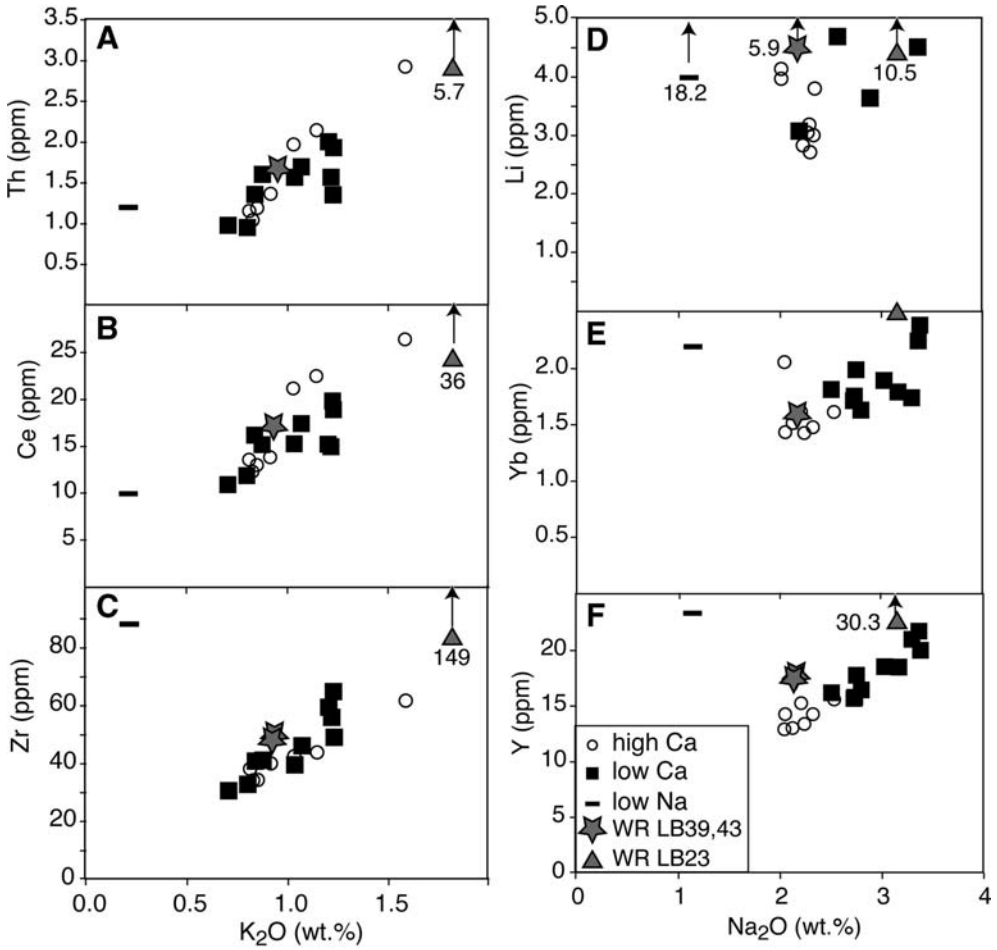

Fig. 8. A–C: Th, Ce and Zr (ppm) versus K_2O (wt.%) of melt inclusions (in olivine $Fo_{88.2–91.2}$, apart for the low-Na inclusion: $Fo_{86.7}$) and WR samples LB23, 39 and 43. The good correlations between incompatible elements with different size/charge ratios suggest a control by partial melting. There is no correlation with the Fo contents of the enclosing olivine. D–F: Li, Yb and Y versus Na_2O content of melt inclusions and whole rocks. Lithium contents were measured on a different group of inclusions than the other trace elements, and show a better (negative) correlation with the CaO content of the enclosing olivine.

inclusion within olivine from mid-ocean ridge basalts (Kamenetsky et al., 1998). The contrast in sodium content between the enclosed melt inclusion and the melt outside the olivine would lead to different CaO partition coefficients between olivine and these contrasting melts (Libourel, 1999). This could then lead to diffusion of Ca from the surrounding melt through the olivine into the melt inclusion. This mechanism is not applicable to the Lombok melt inclusions, as there is no contrast between the Na_2O content of the melt outside the olivine (approximated by the WR Na_2O contents) and that of the melt inclusions. We therefore think that the high CaO contents of the melt inclusions reflect pre-entrapment values of the melt.

Moreover, the trace element patterns of the analysed melt inclusions are very similar to that of the whole rock. Thus, melts similar to those represented by the melt inclusions combined to yield the silicate liquid involved in the whole rock composition. This implies that, at least for this sample, the composition of melt inclusions in $Fo_{89–91}$ olivine can give information on the melts related to the whole rock composition, unlike the situation described for the samples discussed by Danyushevsky et al. (2004).

6.2. Temperature and oxygen fugacity

The common occurrence of spinel crystals enclosed in olivine permits us to use their Fe^{2+}–Mg exchange to determine the equilibration temperature of the magma, using the geothermometer modified from O'Neill and Wall (1987) by Ballhaus et al. (1991a,b, 1994). This

geothermometer is not very pressure-sensitive, and an arbitrary pressure of 0.3 GPa was used for the calculation. Using only spinel–olivine pairs in $Fo_{89–91}$ olivine crystals that had not been reheated for rehomogenisation, calculated temperatures scatter between 986 and 1258 °C, with the bulk lying between 1050 and 1150 °C. There is no relationship between the calculated temperatures and the CaO content of the host olivine. The highest temperatures are likely to be close to the liquidus temperature of the magma, whereas the remainder reflect post-entrapment Fe^{2+}–Mg re-equilibration between olivine and enclosed spinel.

We also approximated the oxygen fugacity of the magma by applying the Ballhaus et al. (1991a) oxygen geobarometer, knowing that this formulation is only strictly valid for assemblages with orthopyroxene, a condition which is not met in our samples. However, the error introduced by the absence of orthopyroxene is rarely more than −0.2 log units (Ballhaus et al., 1991a). For this calculation, we used the temperatures obtained above; the error associated with uncertainty in the temperature is no more than 0.05 log units. The calculated values range from +1.7 to +2.7 log units above FMQ, with the majority between +2.1 and +2.4. This is similar to values for arc peridotites (Parkinson and Arculus, 1999) or for primitive arc magmas (Eggins, 1993). It shows that these calcic melts at least are no different from other types of arc magmas in terms of their oxidation state.

6.3. Volatiles

The measured water contents of the melt inclusions are very low for arc-related magmas, which tend to have more than 1.5 wt.% H_2O in primitive magmas, and up to 10% in more evolved melts (Harris and Anderson, 1984; Sobolev and Chaussidon, 1996; Straub and Layne, 2003; Cervantes and Wallace, 2003; Walker et al., 2003; Wallace, 2005). A rare exception to this rule are the melt inclusions from Galunggung volcano (Java, Indonesia) with water contents around 0.4 wt.% (Sisson and Bronto, 1998). It is noteworthy that these inclusions also have high CaO/Al_2O_3 ratios (Sisson and Bronto, 1998; De Hoog et al., 2001). In our samples, there is one inclusion with significantly higher-water contents than the others (0.7 wt.% versus 0.1 wt.%), but it does not show any major or trace element characteristics that set it apart from the low-H_2O group. This would either point towards highly variable primary H_2O contents, for instance as a result of degassing, or towards variable loss of water after entrapment. The presence of significant CO_2 in the bubbles within melt inclusions, a volatile which is significantly more sensitive to low-pressure degassing than water, suggests that degassing of the melt prior to entrapment into the olivine may not be the cause for the variable water contents measured. There is good evidence that melt inclusions may lose their water on a time scale of hours to days by hydrogen diffusion through the olivine lattice (Hauri, 2002). The fact that many olivine–spinel pairs record temperatures significantly below the crystallisation temperature for these minerals could mean that these crystals spent a prolonged period of time in a crustal magma chamber prior to entrainment to the earth's surface. This sojourn could be the cause of water loss from the inclusions, with the one higher-water inclusion having spent less time within this environment. However, considering the fact that Galunggung high-Ca melts also display low H_2O-contents, it is possible that the measured low H_2O concentrations in our inclusions are real, and are an intrinsic characteristic of nepheline-normative ankaramitic arc magmas.

6.4. Ni content of melt

The Ni contents of magmas can give valuable information on their fractionation stage and the minerals with which they were in equilibrium. Unfortunately, the Ni concentration in the melt inclusions could not be measured directly by electron microprobe using our analytical set-up. We therefore used the NiO-content of the olivine in combination with the major element composition of the melt inclusions to calculate the Ni content of the melt, using the relationship formulated by Beattie (1993). The olivine/melt distribution coefficient for trace elements such as Ni is dependent upon the Fe^{2+}–Mg exchange between olivine and melt, hence this value is influenced by the (recalculation of the) Fe-loss to olivine. We have therefore calculated the Ni content of the melt both with the raw data for the melt inclusions, and with the iron-loss corrected data, assuming a fixed initial FeO content of the melt. The uncorrected data give melt Ni contents between 60 and 160 ppm, the corrected data between 75 and 200, with 230–280 and 365–390 ppm respectively for the melt inclusions within the few olivines with the highest NiO contents of 0.37 wt.% (Fig. 9). Although the absolute values are lower for uncorrected data than for corrected data, the observed trends are similar, with the highest-CaO (lowest-Na_2O) melt inclusions having the lowest Ni contents. This implies that the trends in CaO, Al_2O_3 and Na_2O contents of the melt inclusions cannot be explained by varying degrees of partial melting of a clinopyroxene-rich source, in which case the high CaO

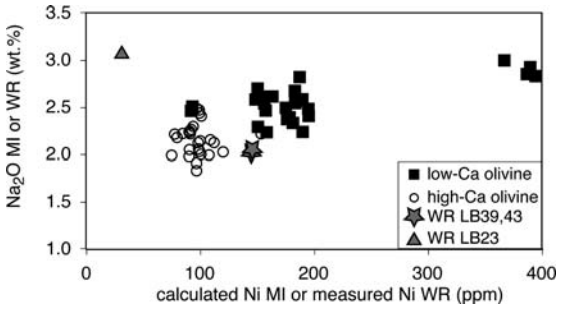

Fig. 9. Measured Na_2O content of melt inclusions and WR samples versus their calculated (MI) or measured (WR) Ni content. Calculation is based on the Ni content of the olivine and the (Fe-loss corrected) FeO and MgO content of the olivine and melt inclusion (Beattie, 1993).

and low Na_2O contents would represent larger degrees of partial melting. This would contradict the lower calculated Ni contents of these CaO-rich, Na_2O-poor melts.

The NiO contents of the high-CaO olivines are much lower than NiO contents of equally Fo-rich olivine phenocrysts in lavas from other tectonic settings, as compiled by Sobolev et al. (2005), but match low Ni contents in olivine from some subduction-related suites, especially those with high-calcium contents (Kamenetsky et al., 1997). The very low NiO-contents of the olivines from the present study could reflect melting of a source in which olivine was extremely stable, resulting in a greatly increased bulk solid/melt distribution coefficient for this element during partial melting (cf. Sobolev et al., 2005). Alternatively, these low Ni contents could mean that the source that melted to form the magma never contained significant amounts of Ni. The possibility that the very high forsterite content, rather than the low Ni content, are a result of unusual circumstances, such as a high fO_2 (Green et al., 2004) is not supported by the olivine–spinel data.

6.5. Major and trace element correlations in melt inclusions

Two correlation trends can be observed within the melt inclusion data (Table 3), which appear to be operating independently of each other. On the one hand, we see a positive correlation between K_2O, Rb, Th, the LREE and Zr (trend 1), which is independent of the CaO content of the melt inclusion, or that of the enclosing olivine (Fig. 8A–C). On the other hand, there is a good positive correlation between Na_2O, Al_2O_3, Y, the HREE and Ni (Fig. 8D–F, 9), and these elements are negatively correlated with the CaO content of the melt inclusion and the enclosing olivine (trend 2).

The similar behaviour of incompatible elements with very different charge/size ratios, and thereby contrasting behaviour during subduction zone enrichment, such as K and Zr (trend 1), is probably best explained by variations in degree of partial melting of the magma source, or fractional crystallisation of a primary magma, or both. Since there is no correlation between these incompatible elements and the forsterite content of the enclosing olivine, which could be taken as a measure of crystal fractionation, we think that these variations are caused by different degrees of partial melting.

We already ruled out variations in degree of partial melting for the trend seen in CaO and associated elements (trend 2) because of the positive correlation between sodium and nickel (Fig. 9). An alternative explanation for this trend is a variation in the chemical or mineralogical composition of the magma source. Considering the disparate chemical behaviour of sodium and yttrium in most environments, the most likely cause of their good correlation is a mineralogical control. Amphibole is one of the minerals that could exert a combined control on Al_2O_3, Na_2O, Y and the HREE. The CaO-related trend observed would then be explained by increasing amounts of amphibole (and thereby decreasing amounts of clinopyroxene) entering into the melt. Although there is some evidence that the solid/melt distribution coefficient for Ni may be larger for amphibole than for clinopyroxene (Dostal et al., 1983), which would explain the increasing amount of Ni in the melt, it is also possible that this Ni-trend comes from a larger contribution of olivine to the melt.

However, the proposed amphibole control on trend 2 does not agree with the very low water contents of the melts. This would imply that the measured water contents are not a primary feature, but reflect hydrogen diffusion out of the glass inclusion. Alternatively, the correlation of Na and Al could reflect a larger jadeite component in the clinopyroxene contributing to the melt. This would also increase the Y and HREE concentrations, as these elements are more compatible in Al-rich clinopyroxene (Wood and Blundy, 2001).

6.6. Petrogenetic model

The interpretation that the composition of the melt inclusions could be explained by varying degrees of melting of a source with a variable mineralogy of clinopyroxene, amphibole and olivine would agree with the experimental work by Médard et al. (2004, 2006). They produced silicate liquids with elemental compositions similar to our high-Ca melt inclusions by melting of a source consisting of olivine, amphibole and clinopyroxene

Table 4
Comparison between experimental and real melt and olivine composition

	Average MI	Experiment
Melt		
SiO_2	45.8	43.9
TiO_2	0.9	2.0
Al_2O_3	13.3	13.8
FeO	9.5	11.8
MgO	10.5	9.3
CaO	16.4	15.6
Na_2O	2.2	2.4
K_2O	0.9	1.1
Olivine		
SiO_2	40.7	39.7
FeO	9.9	15.0
MgO	49.04	44.2
CaO	0.33	0.87

Average MI = an average of Fe-loss corrected melt inclusions in high-calcium olivine of Fo_{89-91}, and average enclosing olivine, from this study. Experiment = Experiment wh08 from Médard et al. (2006) (1300 °C, 1 GPa).

at 0.5–1 GPa and 1175–1350 °C. The liquids which are the best match to our melt inclusions in terms of major element compositions were generated at 1 GPa and 1200–1300 °C (Table 4). Their interpretation is that these calcic liquids found in nature represented remelts of cumulates at shallow levels.

There are, however, two problems with the application of the cumulate–remelting model for the petrogenesis of the Lombok high-calcium melts: the Mg/Fe ratios of the melts, and the isotopic contrast between ankaramites and other lavas from Lombok (see below). The fact that olivine crystals with forsterite contents as high as 91 can crystallise from these calcic melts implies that the melt had very high Mg/Fe^{2+} ratios, and that the source which generated this liquid by partial melting must have had even higher Mg/Fe^{2+} ratios. Note that the experimentally produced olivine does not match the Lombok olivines in terms of Fo-content (Table 4). The spinel–olivine data preclude that the high forsterite contents of the Lombok olivines are the result of exceptionally oxidising conditions during crystallisation. The forsterite contents of the olivines measured are towards the higher end of levels measured in arc magmas in general, and which, in other cases, have been interpreted as reflecting equilibrium with a mantle source (Nakamura, 1995; Kamenetsky et al., 1995; Kamenetsky and Clocchiatti, 1996; Clynne and Borg, 1997; Reubi et al., 2002).

Table 5
Sr, Nd and Pb isotope data for normal and ankaramitic Rinjani (Lombok) samples and samples from Tambora (Sumbawa), previously described by Varne and Foden (1986)

Sample	MgO	CaO/Al_2O_3	$^{87}Sr/^{86}Sr$	2 SE	$^{143}Nd/^{144}Nd$	2 SE	$^{206}Pb/^{204}Pb$	1 SD	$^{207}Pb/^{204}Pb$	1 SD	$^{208}Pb/^{204}Pb$	1 SD
Rinjani normal												
ME01-LB9	5.02	0.55	0.703977*	9			18.673	0.004	15.600	0.003	38.795	0.007
ME01-LB12	3.93	0.51	0.704022	14	0.512855	9	18.667	0.004	15.598	0.003	38.785	0.009
ME01-LB17	5.09	0.56	0.704004	14	0.512881	11	18.670	0.004	15.600	0.003	38.792	0.007
ME01-LB23	4.87	0.57	0.703982	12	0.512871	11	18.669	0.004	15.599	0.003	38.788	0.007
ME01-LB51	5.1	0.57	0.703938*	8			18.700	0.004	15.602	0.003	38.826	0.007
ME01-LB53	3.76	0.4	0.703996*	9	0.512891	9	18.675	0.004	15.607	0.003	38.810	0.007
ME01-LB54	4.63	0.54	0.704011	13	0.512895	9	18.688	0.003	15.604	0.002	38.820	0.006
Rinjani ankaramite Obel–Obel												
ME01-LB36	7.38	0.77	0.704023*	8	0.512853	10	18.786	0.004	15.606	0.003	38.904	0.007
ME01-LB39	10.21	1.03	0.703854*	8			18.726	0.004	15.592	0.003	38.825	0.009
ME01-LB43	11.31	1.03	0.703897	11	0.512861	10	18.725	0.004	15.590	0.003	38.820	0.008
ME01-LB45	6.61	0.71	0.704042	15	0.512830	11	18.795	0.003	15.610	0.003	38.928	0.006
Tambora												
T12	5.22	0.58	0.703915*	7	0.512844	8	18.897	0.003	15.604	0.003	38.957	0.007
T17(48040)	5.56	0.58	0.70389 #		0.512821 #		18.893	0.005	15.601	0.004	38.949	0.009
T23	2.48	0.27	0.703963*	10			18.897	0.004	15.605	0.003	38.969	0.008
T43	2.18	0.23	0.703947*	8			18.899	0.003	15.607	0.002	38.974	0.005
PS4	5.62	0.55	0.703986*	9	0.512791	10	18.802	0.004	15.599	0.003	38.841	0.007

Sr and Nd isotope (normalised to La Jolla = 0.511860) analyses performed at the University of Adelaide, unless stated otherwise. All Pb isotope analyses performed at the Free University, Amsterdam.
* Analyses performed at VU Amsterdam.
# Varne and Foden (1986).

Radiogenic isotope data for whole rocks (Table 5; Varne and Foden, 1986; Turner and Foden, 2001; Paraschivolu and Foden, unpublished data) show a difference between the Lombok ankaramitic series (silica-undersaturated, $CaO/Al_2O_3 > 0.6$) and the other lavas found on the island (Fig. 10). The ankaramites trend towards the fields for the potassic, silica-poor volcanoes Tambora and Sangeang Api on the neighbouring island of Sumbawa. This part of the Indonesian arc has not existed long enough (approximately 10 Ma; Hall, 2002) to explain the differences between Lombok ankaramites and other Lombok lavas by in-situ radioactive decay. If the ankaramitic magmas are generated by remelting cumulates, these cumulates must already have come from a different source than the rest of the magmas from the island. Therefore, the cumulate–remelting model only replaces the problem of finding the source for the high-Ca melts with elucidating the source for the clinopyroxene-rich cumulates.

We therefore propose that the Lombok nepheline-normative ankaramitic melts come from a metasomatised mantle source, consisting of clinopyroxene and olivine, with either amphibole or more jadeitic clinopyroxene as a third component. Garnet involvement to explain the high CaO/Al_2O_3 ratios of the melt (Della-Pasqua and Varne, 1997) is precluded by the flat HREE patterns. An enriched source is supported by the low calculated Ni content of the melt. The high-Ca magma was poor in water, and rich in CO_2, which is in agreement with the silica-undersaturated character of the melts. However, the ankaramitic melts displays the same high LILE/HFSE and LREE/HFSE ratios as normal arc

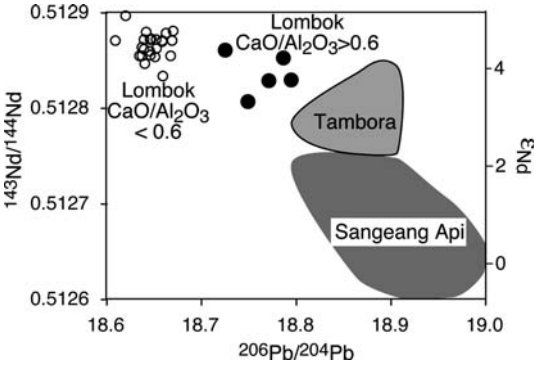

Fig. 10. $^{143}Nd/^{144}Nd$ versus $^{206}Pb/^{204}Pb$ ratio of Lombok whole rocks (Table 5; Varne and Foden, 1986; Foden and Paraschivolu, unpublished data), showing the distinction between the ankaramite-series lavas ($CaO/Al_2O_3 > 0.6$) and the rest of the Lombok samples. Although the Lombok ankaramite data trend towards the fields for Tambora and Sangeang Api volcanoes on the neighbouring island of Sumbawa, the latter are characterised by a significantly more potassium-rich composition than the Lombok ankaramites.

magmas (e.g. sample LB23 in Fig. 7), which argues against the involvement of a $CaCO_3$-rich metasomatic agent only. We may therefore need more than one metasomatic event to explain the source for the ankaramitic magmas.

6.7. Where are the normal basalts?

Inspection of the CaO/Al_2O_3 versus MgO diagram in Fig. 2 shows that all lavas on Lombok with more than 6% MgO belong to what we call the 'ankaramitic series', characterised by increasing CaO/Al_2O_3 ratios with increasing MgO and higher $^{206}Pb/^{204}Pb$ ratios (Fig. 10; Table 5). This highlights the question of why we do not find primitive lavas that could be parental to the non-ankaramitic 'normal' series of magmas on Lombok, and why all primitive lavas, which could, on the basis of their Mg#, have come from the mantle without significant low-pressure fractionation, belong to the ankaramitic series.

It is likely that 'normal' arc magmas are water-rich, whereas ankaramitic magmas contain CO_2 as the dominant volatile. Water saturation inevitably occurs for the normal magma series, resulting in a sudden and dramatic burst of crystal fractionation, which prevents primary magmas from making it to the surface (Tamura and Tatsumi, 2002; Elburg et al., 2006). Degassing of CO_2 does not lead to a significant change in the liquidus temperature of the magma, so ankaramites can make it to the Earth's surface unmodified. If this is true, then ankaramites form a separate magma series, of which the source and the melting processes are different from those that give rise to normal magmas. It means that ankaramites can give little information on the processes that give rise to normal arc magmas and that primitive magmas in arcs will have a disproportionally high chance of being ankaramitic. The nature of the normal arc magmas in Lombok reduces the likelihood of finding their parental magma as a lava flow. Our best hope would be to find melt inclusions in accidentally entrained high-Fo phenocrysts in a more evolved 'normal' magma.

7. Conclusions

The chemical coherence between Fo_{89-91} olivine and enclosed spinel and melt inclusions suggests that they were formed by crystallisation from small individual melt batches. The whole rock composition can be explained by a combination of these melt batches with varying major and trace element concentrations. Therefore, melt inclusions in olivine with forsterite contents greater than 85 mol% can give information about the magma(s)

parental to a whole rock composition. This validates the use of melt inclusions to identify primitive magmas.

The major- and trace elements of the melt inclusions studied are influenced by both the mineralogical composition of the source and the degree of partial melting. The mineralogical control is seen in high contents of Na, Al, Y and HREE for melts with a higher proportion of amphibole or jadeite-rich clinopyroxene, whereas high Ca and Cr contents reflect a higher proportion of jadeite-poor clinopyroxene. Partial melting controls the correlations between LILE, LREE and other incompatible elements.

Considering the high forsterite contents of the olivine and the isotopic distinction between ankaramites and normal basalts, we propose that these ankaramites reflect melting of a subduction-modified, enriched mantle source, rather than remelting of cumulate material.

Acknowledgments

Most of this research was carried out while MAE was a recipient of a European Union Marie Curie Fellowship. VSK was partially funded by a Friedrich Wilhelm Bessel Award (A. von Humboldt Foundation, Germany). Al Hofmann gave MAE and VSK the opportunity to work at the MPI-Chemie in Mainz. Thanks to Ronald Bakker for the Raman spectroscopy analysis of the vapour bubbles. Stephan Klemme helped with the homogenisation experiments in Heidelberg. Andrey Gurenko gave advice on preparation of the melt inclusions, and Nora Groschkopf assisted with electron microprobe analyses. Brigitte Stoll and Kirsten Herweg helped with the LA-ICP-MS analyses. Fun Meeuws is thanked for "proof-reading" of the manuscript. A discussion with Tom Sisson during SOTA-2007 led to some serious rethinking of our initial model. Reviews by Etienne Médard and an anonymous reviewer, and editorial comments by Steve Goldstein helped to improve the focus of the manuscript.

References

Ballhaus, C., Berry, R.F., Green, D.H., 1991a. High pressure experimental calibration of the olivine–orthopyroxene–spinel oxygen geobarometer: implications for the oxidation state of the upper mantle. Contributions to Mineralogy and Petrology 107, 27–40.

Ballhaus, C., Berry, R.F., Green, D.H., 1991b. High pressure experimental calibration of the olivine–orthopyroxene–spinel oxygen geobarometer: implications for the oxidation state of the upper mantle — Erratum. Contributions to Mineralogy and Petrology 108, 384.

Ballhaus, C., Berry, R.F., Green, D.H., 1994. High pressure experimental calibration of the olivine–orthopyroxene–spinel oxygen geobarometer: implications for the oxidation state of the upper mantle — Erratum. Contributions to Mineralogy and Petrology 118, 109.

Beattie, P., 1993. Olivine–melt and orthopyroxene–melt equilibria. Contributions to Mineralogy and Petrology 115, 103–111.

Cervantes, P., Wallace, P.J., 2003. Role of H_2O in subduction-zone magmatism: new insights from melt inclusions in high-Mg basalts from central Mexico. Geology 31 (3), 235–238.

Clynne, M.A., Borg, L.A., 1997. Olivine and chromian spinel in primitive calc-alkaline and tholeiitic lavas from the southernmost Cascade Range, California: a reflection of relative fertility of the source. Canadian Mineralogist 35, 453–472.

Danyushevsky, L.V., Della-Pasqua, F.N., Sokolov, S., 2000. Re-equilibration of melt inclusions trapped by magnesian olivine phenocrysts from subduction-related magmas: petrological implications. Contributions to Mineralogy and Petrology 138, 68–83.

Danyushevsky, L.V., Sokolov, S., Falloon, T.J., 2002. Melt inclusions in olivine phenocrysts: using diffusive re-equilibration to determine the cooling history of a crystal, with implications for the origin of olivine-phyric volcanic rocks. Journal of Petrology 43, 1651–1671.

Danyushevsky, L.V., Leslie, R.A.J., Crawford, A.J., Durance, P., 2004. Melt inclusions in primitive olivine phenocrysts: the role of localized reaction processes in the origin of anomalous compositions. Journal of Petrology 45, 2531–2553.

Davidson, J.P., Hora, J.M., Garrison, J.M., Dungan, M.A., 2005. Crustal forensics in arc magmas. Journal of Volcanology and Geothermal Research 140, 157–170.

De Hoog, J.C.M., Mason, P.R., van Bergen, M.J., 2001. Sulfur and chalcophile elements in subduction zones: constraints from a laser ablation ICP-MS study of melt inclusions from Galunggung Volcano, Indonesia. Geochimica et Cosmochimica Acta 65, 3147–3164.

Della-Pasqua, F., Varne, R., 1997. Primitive ankaramitic magmas in volcanic arcs: a melt-inclusion approach. Canadian Mineralogist 35, 291–312.

Dostal, J., Dupuy, C., Caroon, J.P., Le Guen de Kerneizon, M., Maury, R.C., 1983. Partition coefficients of trace elements: application to volcanic rocks of St. Vincent, West Indies. Geochimica et Cosmochimica Acta 47, 525–533.

Dungan, M.A., Davidson, J., 2004. Partial assimilative recycling of the mafic plutonic roots of arc volcanoes: an example from the Chilean Andes. Geology 32 (9), 773–776.

Eggins, S.M., 1993. Origin and differentiation of picritic arc magmas, Ambae (Aoba), Vanuatu. Contributions to Mineralogy and Petrology 114, 79–100.

Elburg, M.A., Foden, J., 1999. Geochemical response to varying tectonic settings: an example from southern Sulawesi (Indonesia). Geochimica et Cosmochimica Acta 63, 1155–1172.

Elburg, M.A., van Leeuwen, T., Foden, J., 2003. Spatial and temporal isotopic domains of contrasting igneous suites in Western and Northern Sulawesi, Indonesia. Chemical Geology 199, 243–276.

Elburg, M.A., Vroon, P.Z., van der Wagt, B., Tchalikian, A., 2005. Sr and Pb isotopic composition of five USGS glasses (BHVO-2G, BIR-1G, BCR-2G, TB-1G, NKT-1G). Chemical Geology 223, 196–207.

Elburg, M.A., Kamenetsky, V.S., Nikogosian, I., Foden, J., Sobolev, A.V., 2006. Co-existing high- and low-calcium melts identified by mineral and melt inclusion studies of a subduction-influenced syn-collisional magma from South Sulawesi, Indonesia. Journal of Petrology 47, 2433–2462.

Foden, J.D., 1983. The petrology of the calcalkaline lavas of Rindjani volcano, east Sunda arc: a model for island arc petrogenesis. Journal of Petrology 24, 98–103.

Ford, C.E., Russell, D.G., Craven, J.A., Fisk, M.R., 1983. Olivine–liquid equilibria: temperature, pressure and composition dependence of the crystal/liquid cation partition coefficient for Mg, Fe2+, Ca and Mn. Journal of Petrology 24, 256–265.

Gaetani, G., Watson, E.B., 2002. Modeling the major-element evolution of olivine-hosted melt inclusions. Chemical Geology 183, 25–41.

Gaetani, G.A., Cherniak, D.J., Watson, B., 2002. The Reliability of Olivine-Hosted Melt Inclusions: Making Ultracalcic Liquids With a CaO Pump, American Geophysical Union, Fall Meeting 2002, abstract #V21C-02. American Geophysical Union, San Francisco, pp. abstract #V21C-02.

Green, D.H., Schmidt, M.W., Hibberson, W.O., 2004. Island-arc ankaramites: primitive melts from fluxed refractory lherzolitic mantle. Journal of Petrology 45, 391–403.

Gurenko, A.A., Belousov, A.B., Trumbull, R.B., Sobolev, A.V., 2005. Explosive basaltic volcanism of the Chikurachki Volcano (Kurile Islands, Russia): petrology, geochemistry and volatile loading revealed from inclusions in minerals. Journal of Volcanology and Geothermal Research 147, 203–232.

Hall, R., 2002. Cenozoic geological and plate tectonic evolution of SE Asia and the SW Pacific: computer-based reconstructions, model and animations. Journal of Asian Earth Sciences 20, 353–431.

Harris, D.M., Anderson, A.T.J., 1984. Volatiles H_2O, CO_2, and Cl in subduction related basalt. Contributions to Mineralogy and Petrology 87, 120–128.

Hauri, E.H., 2002. SIMS analysis of volatiles in volcanic glasses: 2. Isotopes and abundances in Hawaiian melt inclusions. Chemical Geology 183, 115–141.

Hellebrand, E., Snow, J.E., Hoppe, P., Hofmann, A.W., 2002. Garnet-field melting and late-stage refertilization in 'residual' abyssal peridotites from the Central Indian Ridge. Journal of Petrology 43, 2305–2338.

Jochum, K.P., Stoll, B., Herwig, K., Willbold, M., Hofmann, A.W., Amini, M., Aarburg, S., Abouchami, W., Hellebrand, E., Mocek, B., Raczek, I., Stracke, A., Alard, O., Bouman, C., Becker, S., Dücking, M., Brätz, H., Klemd, R., de Bruin, D., Canil, D., Cornell, D., de Hoog, C.-J., Dalpé, C., Danyushevsky, L.V., Eisenhauer, A., Gao, Y., Snow, J.E., Groschopf, N., Günther, D., Latkoczy, C., Guillong, M., Hauri, E.H., Höfer, H.E., Lahaye, Y., Horz, K., Jacob, D.E., Kaseman, S.A., Kent, A.J.R., Ludwig, T., Zack, T., Mason, P.R.D., Meixner, A., Rosner, M., Misawa, K., Nash, B.P., Pfänder, J., Premo, W.R., Sun, W.D., Tiepolo, M., Vannucci, R., Venneman, T., Wayne, D., Woodhead, J.D., 2006. MPI-DING reference glasses for in situ microanalysis: new reference values for element concentrations and isotope ratios. Geochemistry, Geophysics, Geosystems 7 (2). doi:10.1029/2005GC001060.

Kamenetsky, V., Clocchiatti, R., 1996. Primitive magmatism of Mt Etna: insights from mineralogy and melt inclusions. Earth and Planetary Science Letters 142, 553–572.

Kamenetsky, V.S., Métrich, N., Cioni, R., 1995. Potassic primary melts of Vulsini (Roman Province): evidence from mineralogy and melt inclusions. Contributions to Mineralogy and Petrology 120, 186–196.

Kamenetsky, V.S., Crawford, A.J., Eggins, S., Mühe, R., 1997. Phenocryst and melt inclusion chemistry of near-axis seamounts, Valu Fa Ridge, Lau Basin: insight into mantle wedge melting and the addition of subduction components. Earth and Planetary Science Letters 151, 205–223.

Kamenetsky, V.S., Eggins, S.M., Crawford, A.J., Green, D.H., Gasparon, M., Falloon, T.J., 1998. Calcic melt inclusions in primitive olivine at 43N MAR: evidence for melt–rock reaction/melting involving clinopyroxene-rich lithologies during MORB generation. Earth and Planetary Science Letters 160, 115–132.

Kamenetsky, V.S., Crawford, A.J., Meffre, S., 2001. Factors controlling chemistry of magmatic spinel: an empirical study of associated olivine, Cr–spinel and melt inclusions from primitive rocks. Journal of Petrology 42, 655–671.

Kamenetsky, V.S., Elburg, M.A., Arculus, R.J., Thomas, R., 2006. Magmatic origin of low-Ca olivine in subduction-related magmas: co-existence of contrasting magmas. Chemical Geology 233, 346–357.

Kent, A.J.R., Elliott, T.R., 2002. Melt inclusions from Marianas arc lavas. implications for the composition and formation of island arc magmas. Chemical Geology 183, 263–286.

Libourel, G., 1999. Systematics of calcium partitioning between olivine and silicate melt: implications for melt structure and calcium content of magmatic olivines. Contributions to Mineralogy and Petrology 136, 63–80.

Médard, E., Schmidt, M.W., Schiano, P., 2004. Liquidus surfaces of ultracalcic primitive melts: formation conditions and sources. Contributions to Mineralogy and Petrology 148, 201–215.

Médard, E., Schmidt, M.W., Schiano, P., Ottolini, L., 2006. Melting of amphibole-bearing wehrlites: an experimental study on the origin of ultracalcic nepheline-normative melts. Journal of Petrology 47, 481–504.

Michaud, V., Clocchiatti, R., Sbrana, S., 2000. The Minoan and post-Minoan eruptions, Santorini (Greece), in the light of melt inclusions: chlorine and sulphur behaviour. Journal of Volcanology and Geothermal Research 99, 195–214.

Nakamura, M., 1995. Residence time and crystallization history of nickeliferous olivine phenocrysts from the northern Yatsugatake volcanoes, central Japan; application of growth and diffusion model in the system Mg–Fe–Ni. Journal of Volcanology and Geothermal Research 66, 81–100.

O'Neill, H.S.C., Wall, V.J., 1987. The olivine–orthopyroxene–spinel oxygen geobarometer, the nickel precipitation curve, and the oxygen fugacity of thee Earth's mantle. Journal of Petrology 28, 1169–1191.

Parkinson, I.J., Arculus, R.J., 1999. The redox state of subduction zones: insights from arc–peridotites. Chemical Geology 160, 409–423.

Portnyagin, M.V., Mironov, N.L., Matveev, S.V., Plechov, P.Y., 2005a. Petrology of Avachites, high-magnesian basalts of Avachinsky Volcano, Kamchatka:II. Melt inclusions in olivine. Petrologiya 13 (4), 358–388.

Portnyagin, M.V., Plechov, P.Y., Matveev, S.V., Osipenko, A.B., Mironov, N.L., 2005b. Petrology of Avachites, high-magnesian basalts of Avachinsky Volcano, Kamchatka: I. General characteristics and composition of rocks and minerals. Petrologiya 13 (2), 115–138.

Reubi, O., Nicholls, I.A., Kamenetsky, V.S., 2002. Early mixing and mingling in the evolution of basaltic magmas: evidence from phenocryst assemblages, Slamet Volcano, Java, Indonesia. Journal of Volcanology and Geothermal Research 119, 255–274.

Schiano, P., Eiler, J.M., Hutcheon, I.D., Stolper, E.M., 2000. Primitive CaO-rich, silica-undersaturated melts in island arcs: evidence for the involvement of clinopyroxene-rich lithologies in the petrogenesis of arc magmas. Geochemistry, Geophysics, Geosystems 1 (1999GC000032).

Sisson, T.W., Bronto, S., 1998. Evidence for pressure-release melting beneath magmatic arcs from basalt at Galunggung, Indonesia. Nature 391, 883–886.

Sisson, T.W., Layne, G.D., 1993. H_2O in basalt and basaltic andesite glass inclusions from four subduction-related volcanics. Earth and Planetary Science Letters 117, 619–635.

Sobolev, A.V., 1996. Melt inclusions in minerals as a source of principal petrological information. Petrology 4, 228–239.

Sobolev, A.V., Chaussidon, M., 1996. H_2O concentrations in primary melts from supra-subduction zones and mid-ocean ridges: implication for H_2O storage and recycling in the mantle. Earth and Planetary Science Letters 137, 45–55.

Sobolev, A.V., Hofmann, A.W., Nikogosian, I.K., 2000. Recycled oceanic crust observed in 'ghost plagioclase' within the source of Mauna Loa lavas. Nature 404, 986–990.

Sobolev, A.V., Hofmann, A.W., Sobolev, S.V., Nikogosian, I.K., 2005. An olivine-free mantle source of Hawaiian shield basalts. Nature 434, 590–597.

Straub, S.M., Layne, G.D., 2003. The systematics of chlorine, fluorine, and water in Izu arc front volcanic rocks: implications for volatile recycling in subduction zones. Geochimica et Cosmochimica Acta 67 (21), 4179–4203.

Sun, S.-s., McDonough, W.F., 1989. Chemical and isotopic systematics of oceanic basalts: implications for mantle composition and processes. In: Saunders, A.D., Norry, M.J. (Eds.), Magmatism in the Ocean Basins. Geological Society Special Publication, pp. 313–345.

Tamura, Y., Tatsumi, Y., 2002. Remelting of an andesitic crust as possible origin for rhyolitic magma in oceanic arcs: an example from the Izu–Bonin arc. Journal of Petrology 43, 1029–1047.

Turner, S., Foden, J., 2001. U, Th and Ra disequilibria, Sr, Nd and Pb isotope and trace element variations in Sunda arc lavas: predominance of a subducted sediment component. Contributions to Mineralogy and Petrology 142, 43–57.

Varne, R., Foden, J.D., 1986. Geochemical and isotopic systematics of eastern Sunda Arc volcanics: implications for mantle sources and mantle mixing processes. In: Wezel, F.-C. (Ed.), The origin of arcs. Elsevier, Amsterdam, pp. 159–189.

Walker, J.A., Roggensack, K., Patino, L.C., Cameron, B.I., Matías, O., 2003. The water and trace element contents of melt inclusions across an active subduction zone. Contributions to Mineralogy and Petrology 146, 62–77.

Wallace, P.J., 2005. Volatiles in subduction zone magmas: concentrations and fluxes based on melt inclusion and volcanic gas data. Journal of Volcanology and Geothermal Research 140, 217–240.

Wood, B.J., Blundy, J.D., 2001. The effect of cation charge on crystal–melt partitioning of trace elements. Earth and Planetary Science Letters 188, 59–71.